Article:
Kaskiewicz, PL orcid.org/0000-0001-6708-6687, Rosbottom, I, Hammond, RB et al. (5 more authors) (2021) Understanding and Designing Tailor-Made Additives for Controlling Nucleation: Case Study of p-Aminobenzoic Acid Crystallizing from Ethanolic Solutions. Crystal Growth and Design, 21 (4). pp. 1946-1958. ISSN 1528-7483

https://doi.org/10.1021/acs.cgd.0c01209

Understanding and Designing Tailor-Made Additives for Controlling Nucleation: Case Study of p-Aminobenzoic Acid Crystallising from Ethanolic Solutions

*Peter L. Kaskiewicz†, Ian Rosbottom§, Robert B. Hammond†, Nicholas J. Warren†, Colin Morton§, Peter J. Dowding§, Neil George¥ and Kevin J. Roberts†**

† EPSRC Centre for Doctoral Training in Complex Particulate Products and Processes School of Chemical and Process Engineering, University of Leeds, Leeds, UK

§ Department of Chemical Engineering, Imperial College London, London, UK

§ Infineum UK Ltd, Milton Hill Business and Technology Centre, Abingdon, UK

¥ Syngenta UK Ltd, Jealott's Hill International Research Centre, Berkshire, UK

Keywords

Crystallisation, nucleation, tailor-made additives, nucleation kinetics, crystallisation control workflow, p-aminobenzoic acid

Abstract

A workflow for tailor-made additive screening and crystallisation control using a combination of molecular modelling and experimental techniques is presented. The impact of seven structurally analogous additives, the majority of which containing a carboxylic acid group, on the nucleation of alpha-para-aminobenzoic acid is assessed. Intermolecular grid-search modelling is used to determine dimer interaction energies. Of these, three tailor-made additives are found to form stronger carboxylic group dimer interactions with the compound. Solvation energy calculations demonstrate the stability of these dimers in solution. Subsequent intermolecular interaction assessment demonstrates an ability of one of the tailor-made additives to interfere with the molecular preassembly route to nucleation, with molecular charge distributions providing an insight into this effect. Polythermal crystallisation experimental screening confirms the effectiveness of these tailor-made additives to inhibit nucleation. Interestingly, the nucleation mechanism is found to change from instantaneous to progressive nucleation in the absence and presence of the tailor-made additives in solution, respectively, together with an increase in the effective interfacial tension.

1. Introduction

Crystallisation is a process that is extensively utilised in industry to produce a pure and stable solid form with defined physical and chemical properties. It is also, under certain conditions, an inevitable natural process that cannot be avoided, even when it is not desirable. To this latter end, steps can be taken to try and inhibit unwanted crystallisation, through e.g. solvent selection, to try and gain greater 'control' over the crystallisation processes to alter solubility[1], crystallisability[2], polymorphic[3–5] or solvated forms[6], etc. Additives are also often employed to aid in the control of crystallisation events[7].

The ability of additives to interfere with the crystallisation process has been well studied with respect to both inorganic[8–11] and organic[12–17] systems, as well as utilising computational modelling methodologies to try and understand their effect at a molecular level[18–20]. Studies on the influence of additives on the crystallisation process have focused heavily on tailor-made additives (TMAs), which refer to compounds added to a crystallisation system that act as imposter molecules, having only slight differing moieties than the solute to be crystallised, and as such, a similar molecular structure to the target solute[17]. TMA research has concentrated on their effect on crystal growth[18,19,21–23], however, their effect on the nucleation process has been an area of growing focus. These additives have the capacity to disrupt/aid the nucleation process by interacting with nuclei cluster formation and/or cluster reorientation[24–27]. However, the process by which this can occur is extremely complex.

Although research into the effects of TMAs on nucleation has become a more prominent area of study[28], TMA selection can still be a somewhat empirical approach, whereby nucleation inhibition TMAs may be selected for study based on their molecular structure alone. However, this does not take into account the structural arrangement and binding energetics associated with the specific intermolecular (synthonic) interactions, relating to the nucleation stage of crystallisation. Such knowledge can greatly enhance understanding of how specific molecular moieties can disrupt nucleation, hence providing a resource and workflow for crystallisation process design. On a fundamental level, this can also give an indication into which solute:solute interactions are dominant in the pre-nucleation clustering process. Reflecting this, we introduce an in silico TMA screening tool that, whilst being computationally efficient, can provide an insight into both the relative strength of solute:solute and solute:TMA intermolecular interactions respectively, as well as their structural orientation in space, which when integrated with crystallographic structure can provide valuable insight into TMA effectiveness.

Grid-based molecular modelling tools have been successfully utilised for a number of fundamental crystallisation studies[20,29–35], including studies of the interaction of solvent molecules with pABA to aid in solvent selection and crystallisation process design[36]. In this paper, the grid-search approach has been used to understand the dominant molecular interactions between pABA and the TMAs, in terms of their synthonic interaction structures and energetics.

An experimental polythermal assessment was utilised for validation of in silico results and to provide insight into TMA influence on the nucleation process. The crystallisability, in terms of the steady-state metastable zone width (MSZW) to crystallisation as well as solution thermodynamics

were assessed. These factors have previously been studied to gain an understanding of the effects of varying solvents and solute compositions on the crystallisation process[2]. The Kashchiev-Hammond-Borissova-Roberts (KBHR) approach[37–39], which has been used in a number of research studies, was employed to determine nucleation kinetic parameters and distinguish the mechanism by which the solutions nucleated, either through instantaneous or progressive nucleation (IN or PN, respectively). IN describes the process in which all nuclei form instantly and subsequently undergo crystal growth, whereas in PN nuclei continuously form in the presence of growing crystals.

This work focusses on a case study of the nucleation of p-aminobenzoic acid (pABA), figure 1, from ethanol solution, in the presence of a selection of TMAs. pABA was selected for this study due to its functional groups being representative of many pharmaceutical compounds and is well studied in terms of polymorphism[40–44], morphology[45,46], solution structure[6,36,47–49], TMAs[27], nucleation[1,50–53] and growth[54]. A previous study by Black et al.[27] focused on the influence of two TMAs, 4-amino-3-methoxybenzoic acid (AMBA3), and 4-amino-3-nitrobenzoic acid (ANBA3), on pABA crystallisation and found that they were able to lower both the nucleation and growth kinetics, as well as direct polymorphic forms at a given solution scale. This work takes on a synthonic engineering perspective[55] and aims to more thoroughly elucidate the specific intermolecular interactions underpinning the ability of TMAs to disrupt pABA nucleation as well as provide a standardised TMA assessment procedure through the tools used in this study. In order to aid future studies in the area of TMA assessment and understanding, a multilayer workflow is presented.

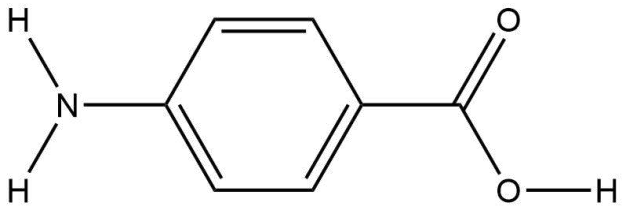

Figure 1. Molecular structure of p-aminobenzoic acid.

2. Workflow, Materials & Methods

A methodological workflow outlining the proposed steps for simple nucleation inhibition TMA screening and assessment, using the tools outlined in this work, is provided in figure 2. This workflow was developed and utilised for TMA screening and assessment and is presented in order to try and aid future TMA selection and understanding. The stages presented outline the structure of the materials & methods and results & discussion sections of this article.

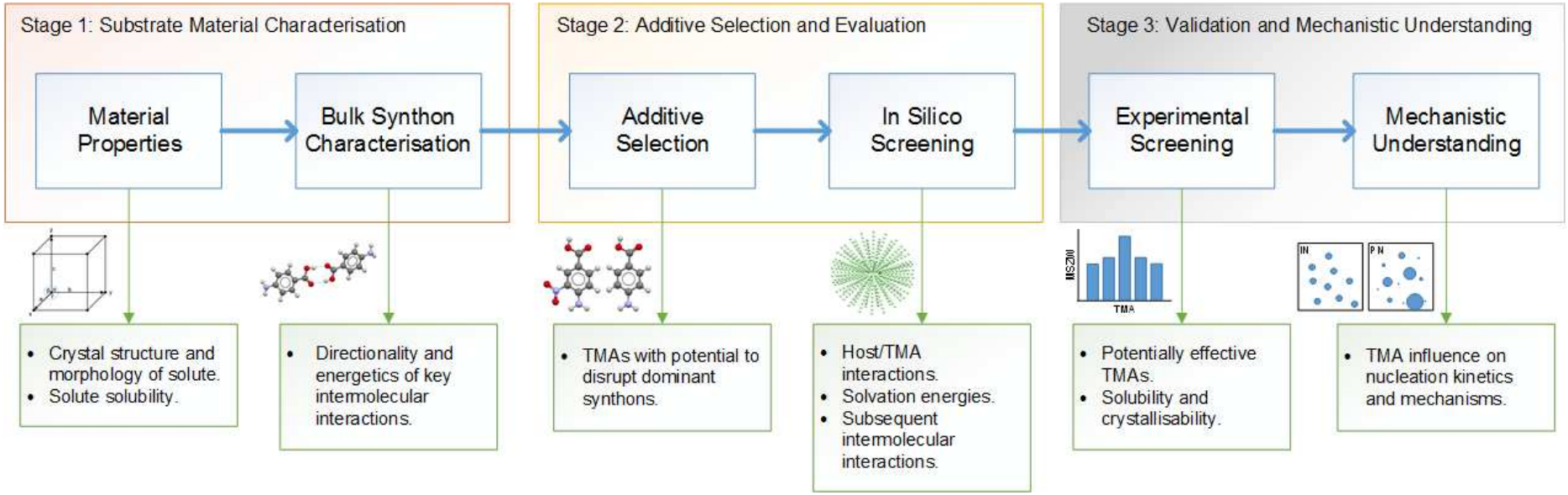

Figure 2. Diagrammatic workflow outlining key steps involved in TMA screening and assessment.

2.1. Material Properties & Bulk Synthon Characterisation

Material selection for TMA assessment in industrial environments is often dominated by product development, which dictates the solute that is studied. Knowledge of basic material properties of the target solute, such as crystal structure, morphology and solubility must be gained to optimise process design and aid in TMA assessment.

Knowledge of key synthons within the solute crystal structure can be obtained through experimental and/or computational material property assessment to determine key crystallographic data or through prior research/crystal databases, such as the Cambridge Structural Database (CSD)[56].

2.2. Additive Selection

In order to ensure experimental validation and assessment could take place, TMAs that were commercially available were used in this study. The criteria for TMA selection focussed upon molecular similarity to pABA as well as the bulk synthonic characterisation results, whereby TMAs were selected that could have potential strong intermolecular interactions with the dominant synthons present in the pABA crystal structure.

2.3. In Silico Screening

2.3.1. Calculation of TMA Interaction

Intermolecular grid searches were performed by using the molecular interaction energy predictor, available within the VisualHABIT synthonic engineering tool set[30]. These searches took

pABA as the target molecule, centred around which a 3D spatial grid was defined, and a probe molecule (pABA or a TMA). A spherical grid with radius of 15 Å from the target molecule (pABA) with 10 steps of grid points on the radius, the polar angle and on the equator, provided a grid with total points of 921, which was defined for energy calculations. A description of the grid optimisation procedure used as well as visualisations of the grid are given in Supplementary Information S2. At each point on the grid, the probe molecule was placed and rotated through a grid of Euler angles, which were set at 4º for the x-axis, y-axis and z-axis. This resulted in a heterogeneous six dimensional search space, and at each point in this search space the interaction energy of the probe and target assemblies was calculated using the Dreiding[57] potential. All grid based intermolecular interaction calculations were performed using a standard PC with CPU times in the range of minutes and hours.

Atomic fractional charges were derived from a calculation of the electrostatic potential at the density functional theory, using a 6-31G* basis set and the Becke three-parameter[58], Lee-Yang Parr exchange-correlation function[59], using Gaussian09[60]. This was completed using high performance computing with CPU times of less than one hour for each molecule studied.

Intermolecular interactions in the form of van der Waals, hydrogen bonding and electrostatic interactions were calculated. The strongest intermolecular interactions for pABA:pABA and pABA:TMAs were compared and the target and probe assemblies for the strongest interactions predicted were assessed, in terms of their geometrical arrangement, using the Biovia Materials Studio[61] software package to visualise the most prominent molecular interaction orientations.

The subsequent most energetically favourable dimer structures of each interaction pair were used to calculate the likely interactions of further pABA molecules. Five pABA molecules were used as probes, with the dimers used as the grid search target structures. The same grid dimensions and Euler angles, as well as interaction energy and interaction geometry assessment method, as aforementioned, were used.

2.3.2. Calculation of Solvation Energies

The intermolecular grid search method was also used to calculate the solvation energies of the most energetically favourable dimer structures determined from the pABA:pABA/TMA intermolecular interaction calculations. Twenty ethanol molecules were used as the probes, providing enough solvent molecules to ensure the target dimers were well solvated. A slightly smaller grid size of 14 Å with 9 steps of grid points on the radius, the polar angle and on the equator, was used, slightly reducing the number of grid points to enable the software to calculate interactions with the high number of probe molecules. Further optimisation of the calculated interaction shell, using the Forcite module within Biovia Materials Studio was performed. The SMART algorithm and a very fine tolerance was used to distinguish intra and inter-molecular interactions, ensuring solvation energies alone could be determined. For this, Gasteiger[62,63] atom point charges were utilised.

2.4. Experimental Screening

2.4.1. Materials

pABA, 3-aminobenzoic acid (mABA) and 4-nitrophenol (pNP) were supplied by Alfa Aesar, 4-amino-3-methoxybenzoic acid (AMBA3), 4-amino-2-methoxybenzoic acid (AMBA2), 4-amino-3-nitrobenzoic acid (ANBA3) and 4-amino-2-nitrobenzoic acid (ANBA2) were supplied by Fluorochem, 4-aminosalicyclic acid (pASA) was supplied by LKT Laboratories Inc. and ethanol absolute was supplied by Sigma-Aldrich. All materials were used as received without further purification.

2.4.2. Experimental Procedure

All experiments were performed using the Technobis Crystal16 system[64] at a 1 ml solution scale.

A TMA screen was performed through determination of changes in solution crystallisation temperature (T_c) in the presence of TMAs, using a polythermal analysis[2]. Solutions at a concentration of 0.17g (99 mol% pABA: 1 mol % TMA) g^{-1} ethanol were subjected to heating cycles at a rate of 0.5 °C min^{-1} between 37 °C and -15 °C, with constant magnetic stirrer bar agitation at 300 rpm. Temperature cycles were repeated 12 times to get average T_c and dissolution temperatures (T_{diss}). T_c and T_{diss} were determined through transmissivity data as a function of temperature, as described in a previous research article[2].

2.5. Mechanistic Understanding

The most effective TMA was further analysed and compared to the crystallisation of pABA from ethanol solution. Steady-state metastable zone width (MSZW) analysis, van't Hoff analysis and nucleation kinetic analysis through the KBHR approach, subsequently described, were performed. pABA in ethanol at concentrations of 0.14, 0.15, 0.16 and 0.17 g g^{-1} and pABA:TMA (99:1 mol%)

in ethanol at concentrations of 0.18, 0.19, 0.20 and 0.21 g g^{-1} were studied. Heating cycles at rates of 0.3, 0.5, 0.7 and 0.9 °C min^{-1} in the temperature range 37 °C to -15 °C were used with a minimum of 5 repeats for pABA in ethanol solutions. For pABA:TMA in ethanol solutions, additional heating cycle rates of 0.4, 0.6 and 0.8 °C min^{-1} were used. T_c, T_{diss}, the equilibrium crystallisation temperature at the kinetic limit ($T_{c/l}$) and the equilibrium dissolution temperature (T_e) were determined as described elsewhere[2]. The difference between $T_{c/l}$ and T_e provided the steady-state MSZW.

A van't Hoff analysis was performed from the obtained solubility data to determine how the systems of study deviated from ideality, with the ideal solubility of pABA obtained from previous literature[49]. Activity coefficients (Υ), enthalpy (ΔH_{diss}) and entropy (ΔS_{diss}) of dissolution were calculated based on the following equations[65,66]:

$$\ln(x_{ideal}) = \frac{\Delta H_{fus}}{R}\left[\frac{1}{T} - \frac{1}{T_m}\right] \quad (1)$$

$$\Upsilon = \frac{x_{ideal}}{x} \quad (2)$$

$$\ln(x) = -\frac{\Delta H_{diss}}{RT} + \frac{\Delta S_{diss}}{R} \quad (3)$$

Where x_{ideal} is the solution concentration, x is the experimentally measured mole fraction, ΔH_{fus} is the enthalpy of fusion, R is the ideal gas constant, T is the temperature and T_m is the melting temperature.

The KBHR approach was undertaken to gain an insight into the mechanism by which pABA:TMA in ethanol solutions nucleated in comparison to pABA in ethanol solutions, as well

as to determine nucleation kinetic parameters to assess changes in the effective interfacial tension (γ_{eff}) to nucleation, giving an insight into the ease by which the systems crystallised. The KBHR approach relates the relative critical undercooling (u_c) to the cooling rate (q), utilising classical nucleation theory (CNT). u_c was calculated through the relationship:

$$u_c = \frac{\Delta T_c}{T_e} \qquad (4)$$

Where, $\Delta T_c = T_e - T_c$

Plots of u_c vs q in ln-ln coordinates were produced, with slopes of fitted linear regressions providing information as to the mechanism of nucleation. A slope <3 indicated an instantaneous nucleation pathway, whereas a slope >3 signified a progressive nucleation pathway. IN describes the pathway by which all nucleation active sites in a system (in this case a solution) have practically equal activities. Therefore, when a level of supersaturation is reached, corresponding to the critical level of supersaturation required for nucleation, all nucleation events occur at one instance. In contrast, PN describes the pathway by which nucleation active centres have a range of activities and therefore this non-uniform distribution of energies results in nucleation events occurring over a range of time, once individual nuclei reach the critical cluster size required for nucleation, where nucleation events can take place in the presence of already growing crystals.

For the case of PN, The final expression for $u_c(q)$ dependence, when expressed through the number of crystallites at the detection point (N_{det}), is defined as:

$$\ln q = \ln q_0 + a_1 \ln u_c - \frac{a_2}{(1-u_c)u_c^2} \qquad (5)$$

Plots of u_c vs. ln q fitted with equation 5 enabled parameters to be determined for the calculation of the nucleation kinetic parameters of γ_{eff}, the critical nucleus radius (r^*) and the number of molecules in the critical nucleus (i^*).

A full description of the KBHR analysis approach methodology is outlined in a previous research article[39].

3. Results & Discussion

3.1. Material Properties

pABA has a number of polymorphic forms, but has two major polymorphs, α- and β-pABA, with α-pABA being the most commonly observed form. This paper concerns the α-polymorph, which is subsequently referred to simply as pABA. pABA crystallises in the monoclinic crystal system, with space group $P2_1/n$ and 2 molecules in the asymmetric unit. The mix of polar and apolar structural groups of pABA, as well as the structurally distinct polymorphs with very different physical properties, make this an attractive model compound. The needle-like alpha form of pABA often dominates the crystallisation from organic solvents and has been shown to be highly soluble in ethanol[48].

3.2. Bulk Synthon Characterisation

Synthon analysis of pABA has been previously studied, with the results summarised here. The solid-state packing of pABA is made up of -O-H···O- dimer hydrogen bonding (synthon A), head-to-head π-π stacking of the phenyl rings (synthon B) and amine to carboxylic group -N-H···O-

hydrogen bonding (synthon C) synthons (figure 3)[46]. Several studies of the nucleation rates in different solvents and pre-nucleation structure has indicated that the desolvation of the carboxylic acid group, along with the subsequent formation of the pABA:pABA OH…O H-bond, is an important step for the nucleation of the alpha-form[45,47,48,52,67]. However, computational and experimental studies in water and nitromethane have implied that disruption of the π-π stacking interactions can also impact upon the nucleation behaviour of pABA[6,27,51] and may be the dominant synthon type in controlling the nucleation of pABA from solution[27,51]. Although there is evidence to support both the synthon A and the synthon B hypothesis for pABA nucleation control, open literature is more suggestive of synthon A dominance in ethanol solution, which is the basis of the work presented in this paper. A thorough discussion on these contrasting views in provided in Supplementary Information S1.

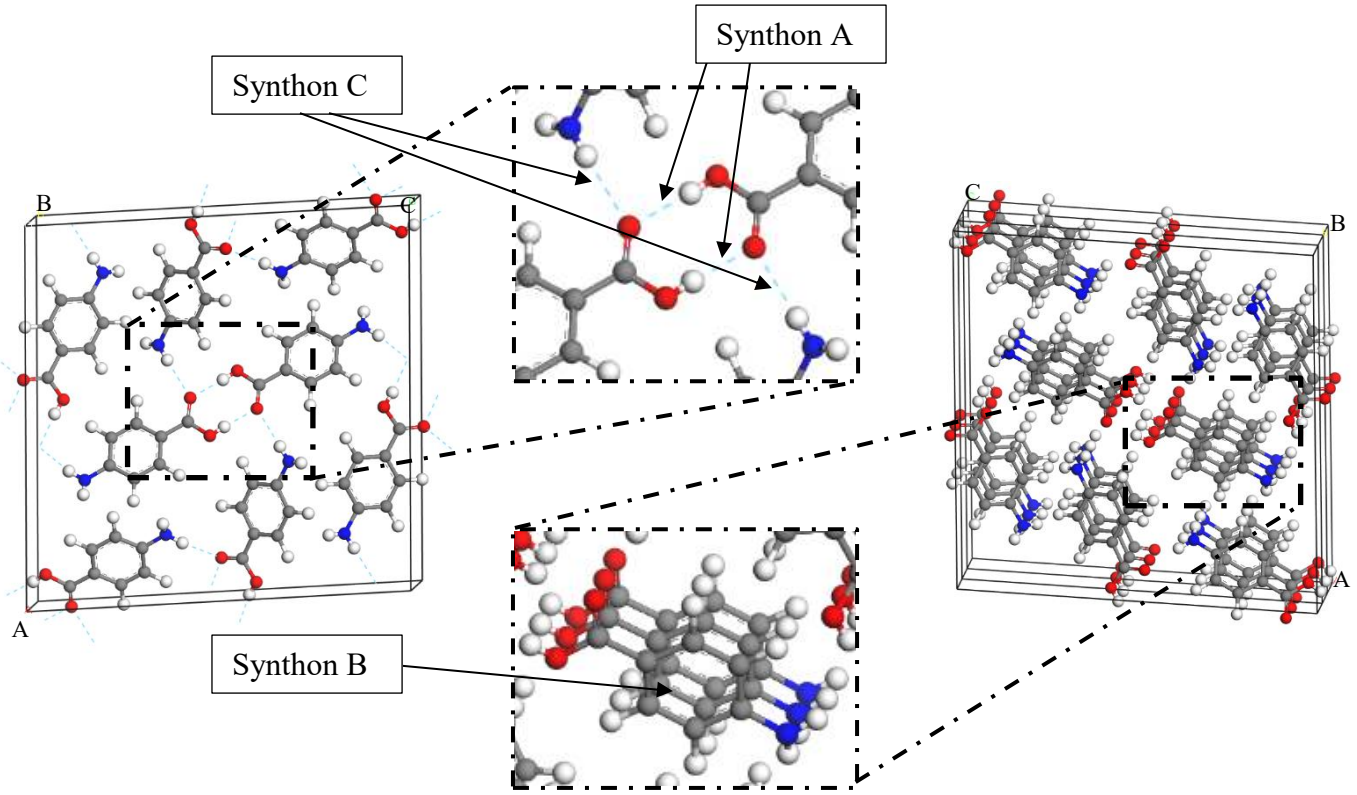

Figure 3. pABA crystal structure. Left-hand side - pABA unit cell, showing carboxylic dimer -O-H···O- hydrogen bonding (synthon A) and -N-H···O- hydrogen bonding (synthon C). Inset shows dominant hydrogen bonding tetramer intermolecular interactions. Blue dashed lines show intermolecular hydrogen bonding. Right-hand side - pABA structural packing in the c-axis, showing π-π stacking of the cyclic rings of pABA (synthon B). Inset highlights π-π stacking. Taken from AMBNAC07 in Cambridge Structural Database[46].

3.3. Additive Selection

Potential nucleation inhibition additives were selected based on two factors. Firstly, in order to meet the criteria of being termed TMAs, as outlined by the seminal work of the Weizmann Institute[17], additives that had molecular similarity to pABA were selected. Also, knowledge gained from the aforementioned pABA bulk synthon characterisation[45] was used to aid selection of TMAs that could potentially impact upon the important pABA crystallographic synthons, i.e. through exploiting electrostatic or steric hindrance effects, in an effort to inhibit nucleation. The molecular structures of pABA and all TMAs studied are given in figure 4.

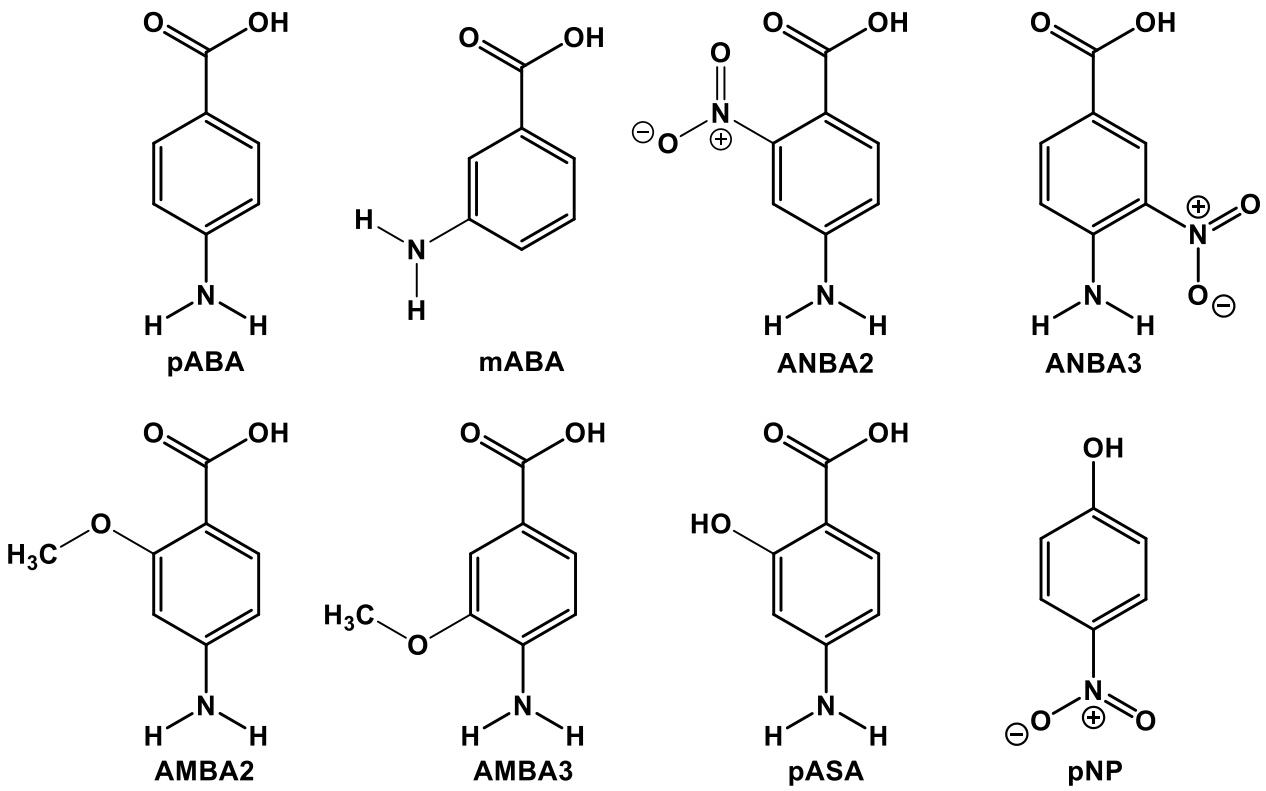

Figure 4. Molecular structures of pABA and the selection of seven TMAs, which are closely related in their molecular structure to pABA.

3.4. In Silico Screening.

3.4.1. In Silico Intermolecular Grid Search TMA Screen - Dimers

A comparison of the strongest intermolecular interaction energy values, determined from the grid-search analysis, between pABA:pABA and pABA:TMAs is summarised in table 1. The variation in calculated intermolecular interaction energies were found to be relatively small between the dimer interactions, except for pABA:pNP, which showed a larger variation. Given that the same calculation procedure was undertaken for all intermolecular interaction calculations

and all TMAs, except pNP, had strong interacting carboxylic and amine groups, these calculated values were taken to provide a trend in intermolecular interaction strengths between pABA:pABA and pABA:TMAs.

The data indicates that for pABA:ANBA3, pABA:AMBA2 and pABA:AMBA3 intermolecular interactions energies were calculated to be stronger (more negative) than for those of pABA:pABA. We theorise that the stronger binding of these structurally related TMA's may disrupt the formation of a critical sized nucleus for pABA nucleation. In contrast, the other tested TMAs were calculated to bind more weakly with pABA and thought to be less likely to inhibit nucleation. No significant changes were observed in trends for decreasing pABA:TMA interaction energies over the range of interactions calculated. An analysis of over 3000 calculated intermolecular interaction energies for each pABA:TMA system, as well as pABA:pABA, is provided in Supplementary Information S3.

Table 1. Strongest interaction energies for pABA:pABA and pABA:TMA from intermolecular grid search along with Van der Waals, hydrogen bonding and electrostatic interaction contributions to total energy.

Molecule in dimer with pABA	**Van der Waals interaction energy (kcal mol^{-1})**	**Hydrogen bonding interaction energy (kcal mol^{-1})**	**Electrostatic interaction energy (kcal mol^{-1})**	**Total interaction energy (kcal mol^{-1})**	**% Variation in total interaction energy compared to pABA:pABA**
pABA	0.80	-5.33	-4.50	-9.03	0.00
mABA	1.35	-5.50	-4.81	-8.96	+0.78
ANBA2	1.02	-4.74	-5.21	-8.93	+1.11
ANBA3	1.16	-5.84	-4.71	-9.39	-3.99
AMBA2	1.25	-5.63	-4.93	-9.31	-3.10
AMBA3	1.89	-5.63	-5.54	-9.28	-2.77
pASA	1.27	-5.13	-5.16	-9.02	+0.11
pNP	0.68	-4.06	-3.40	-6.78	+24.92

For the strongest intermolecular interaction energies calculated, hydrogen bonding tended to be the dominant intermolecular interaction type, with a high electrostatic contribution and a low/repulsive Van der Waals contribution to the overall intermolecular interaction energies calculated, which matched the trend observed for pABA:pABA and suggested strong hydrogen bonded carboxylic group dimer formation (synthon A).

The most energetically favourable intermolecular interaction geometries of pABA:pABA, pABA:ANBA3, pABA:AMBA2 and pABA:AMBA3 are displayed in figure 5. All strongest

calculated interactions were the OH…O H-bonding dimer, which is analogous to the strongest synthon in the alpha pABA structure (synthon A). This suggests that ANBA3, AMBA2 and AMBA3 are able to disrupt the important pABA:pABA dimer formation, which has been experimentally suggested to form prior to nucleation of alpha pABA and template the self-assembly of this structure[48]. For all pABA:TMA intermolecular interactions studied, synthon A was found to be the most energetically favourable interaction type, with the exception of pABA:pNP, due to pNP lacking the carboxylic acid group moiety. This similarity across the interactions studied also highlights the relatively small changes in intermolecular interaction energies calculated for these systems. It also suggests that energy scaling/normalization based on molecular size would not be necessary for a comparison of interaction energies, as all interactions, except for pABA:pNP, were the same type. The most favourable interactions calculated for each pABA:TMA are given in Supplementary Information S5.

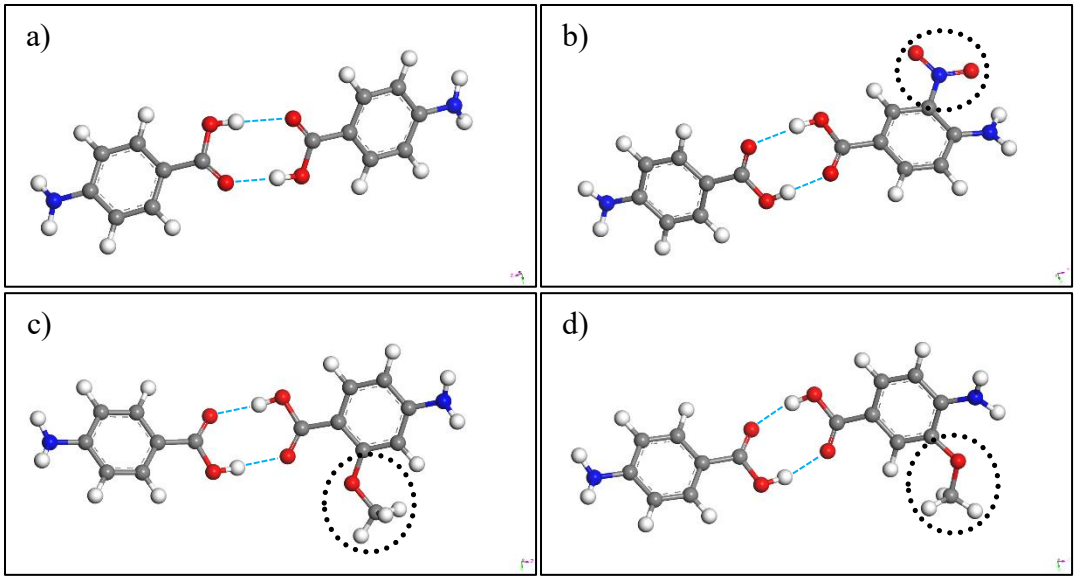

Figure 5. Most favourable interactions of a) pABA:pABA, b) pABA:ANBA3, c) pABA:AMBA2 and d) pABA:AMBA3, calculated from intermolecular grid search. Hydrogen bonding shown by blue dashed lines. Additional functional groups of TMAs are highlighted in the dotted circles.

3.4.2. In Silico Intermolecular Grid Search TMA Screen - Solvation

The calculated solvation energies of the most energetically favourable calculated dimers of pABA:pABA, pABA:ANBA3, pABA:AMBA2 and pABA:AMBA3 are given in table 2.

All potential most energetically favourable pABA:TMA dimers were found to be more strongly solvated than the pABA:pABA dimer. This is likely due to the additional moieties on the TMA molecules, which enabled stronger interactions with the ethanol molecules. The strongest solvation energy of the three determined most likely pABA:TMA dimers was pABA:ANBA3. A stronger solvation demonstrates that the dimers would be more stable within solution and would be harder

to desolvate for subsequent pABA intermolecular interactions to take place through the key secondary synthons B and C, making nucleation more difficult.

Table 2. Solvation energies of 20 ethanol molecules interacting with pABA:pABA and pABA:TMAs.

Molecule in dimer with pABA	**pABA**	**ANBA3**	**AMBA2**	**AMBA3**
Solvation Energy (kcal mol^{-1})	-58.71	-76.03	-60.43	-73.52

3.4.3. In Silico Intermolecular Grid Search TMA Screen – pABA Interactions with Stable Dimers

For 5 pABA molecules interacting with the studied dimers, the total interaction energies calculated with the pABA:TMAs were found to be stronger than with of pABA:pABA. This is consistent with the ethanol solvation results and is again likely due to the additional moieties of the TMAs having an effect on the oriented intermolecular interactions of pABA with the dimers. Therefore, intermolecular interactions of pABA molecules with the dimers in solution would be more favourable with the pABA:TMA dimers than with the pABA:pABA dimer. This suggests that if the TMAs were required to be removed from the prenucleation clusters in order for the pABA crystal structure to form and nucleation to occur , more energy would be required to achieve this. This mechanism of nucleation inhibiting additives being required to be removed from the prenuclei to enable nucleation to occur has been suggested in previous literature[24]. The

intermolecular interaction energies calculated for 5 pABA molecules interacting with all pABA:pABA and pABA:TMA dimers are given in Supplementary Information S7.

The interaction geometries of the 5 pABA molecules with the most stable pABA:pABA dimer and the three most stable pABA:TMA dimers (ANBA3, AMBA2 and AMBA3) are displayed in figure 6. These geometries provide information as to the likely effect of the important secondary synthonic interactions of pABA necessary for nucleation in ethanol solution to occur. For pABA molecules interacting with the pABA:pABA, pABA:AMBA2 and pABA:AMBA3 dimers, the strongest intermolecular interaction was synthon C, with the amine group of the pABA molecule interacting with the carboxylic acid groups of the dimers. This relates strongly to the pre assembly mechanism of pABA. In contrast, the strongest intermolecular interaction with a pABA molecule and the pABA:ANBA3 dimer does not relate to the important secondary synthons B or C. Instead, the amine group of the interacting pABA molecule interacts with the nitro group of ANBA3, directing strong non-crystallographic synthons. This suggests that ANBA3 has the strongest pABA nucleation inhibition capabilities of any of the TMAs studied, with its meta-position nitro group having a large effect on the ability of pABA molecules to form key synthonic interactions and nucleate.

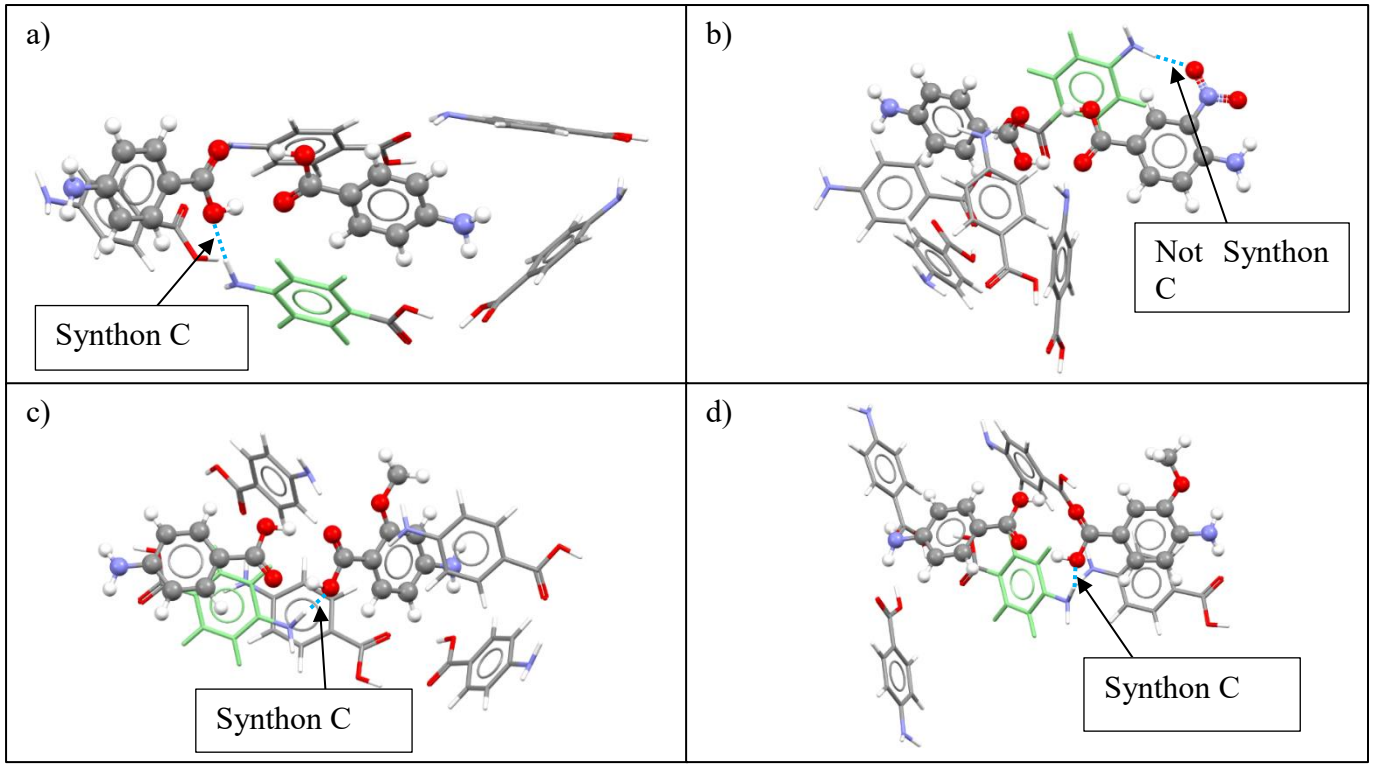

Figure 6. Interaction clusters of 5 pABA molecules around the calculated most energetically favourable (a) pABA:pABA, (b) pABA:ANBA3, (c) pABA:AMBA2 and (d) pABA:AMBA3 dimers. Dimers are shown with ball and stick style. pABA probe molecules are shown with capped stick style. Strongest pABA intermolecular interactions with each dimer are shown with pABA molecules with light green cyclic rings. Blue dashed lines represent intermolecular hydrogen bonding for strongest pABA interaction with dimer.

3.4.4. In Silico Intermolecular Grid Search TMA Screen – Atomic Charges

The calculated fractional charges of atoms on ANBA3, AMBA2 and AMBA3, figure 7, provide further insight into the possible pABA nucleation inhibition effect of these TMAs. Charges calculated over the nitro group on ANBA3 ranged from 0.69 to -0.45, whereas the methoxy group charges of AMBA2 and AMBA3 ranged from -0.28 to 0.02. The larger charges of the nitro group suggest that ANBA3 would have a stronger influence on ethanol and pABA molecules within solution than AMBA2 or AMBA3, as seen in the solvation and pABA cluster results. A comparison of atomic charges of pABA and the selected TMAs shows somewhat minor variations in charges on amino groups of the molecules, except for ANBA3, which showed a large change in atomic charges. The nitro group of ANBA3 has strong electron withdrawing capacity towards the amino group and as such, created more positively charged hydrogen atoms and a more negative nitrogen atom (figure 7). The higher positive charges of the amino group hydrogen atoms of ANBA3 would create stronger -N-H⋯O- intermolecular interactions with subsequent pABA molecules, and as such could potentially disrupt the pre-assembly/nucleation pathway required for nucleation of pABA from ethanol solution more than for the other TMAs studied. Therefore, it would be expected that ANBA3 would be a more effective TMA for pABA nucleation inhibition from ethanol solution than AMBA2 and AMBA3.

The charges on the cyclic rings of the TMAs were also influenced by the additional functional groups present, compared to the pABA molecule, with subtle changes in the calculated charges of the carbon atoms. These charges influence the π-π stacking synthon B interactions and as such, it is likely that the changing polarizability would influence this synthon, however, it is less clear at this stage as to the exact influence these changes would have on synthon B formation. Nevertheless, a previous study found that the synthon B interaction of both ANBA3

and AMBA3 with a pABA molecule is stronger than that of pABA with another pABA molecule, although the geometries of these interactions altered significantly from the pABA crystallographic solid state synthon B[27].

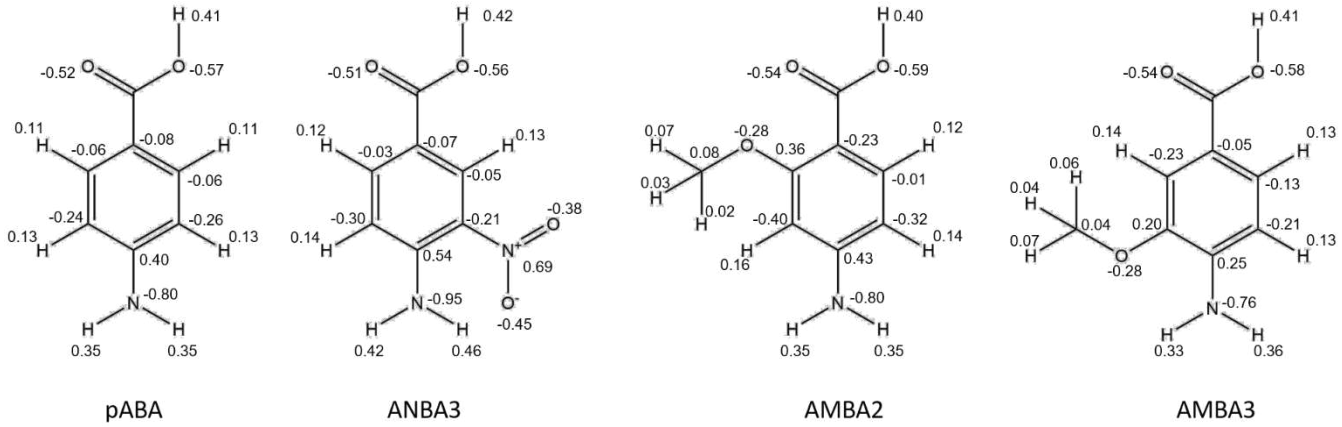

Figure 7. Fractional charges calculated for each atom of pABA, ANBA3, AMBA2 and AMBA3.

3.4.5. In Silico Intermolecular Grid Search TMA Screen –TMAs in pABA Crystal Structure

To further aid conceptualisation of how these TMAs could potentially inhibit formation of the pABA crystal structure, figure 8 displays visualisations of the strongest interactions of pABA:TMAs, taken from figure 6, within the pABA unit cell structure[46]. These TMAs could have a significant effect on disrupting the pABA crystal structure formation through electrostatic and steric hindrance towards subsequent pABA molecules joining the strong dimer formed in ethanol solution. The additional nitro moiety of ANBA3 and the methoxy moieties of AMBA2 and AMBA3 could disrupt pABA molecules orientating into the required crystal structure and inhibit the important crystallographic synthon B formation. Given that the nitro group is a larger moiety than the methoxy group, ANBA3 would have a larger disruptive effect

on crystal structure formation. A space fill figure is provided in Supplementary Information S8 to further highlight this.

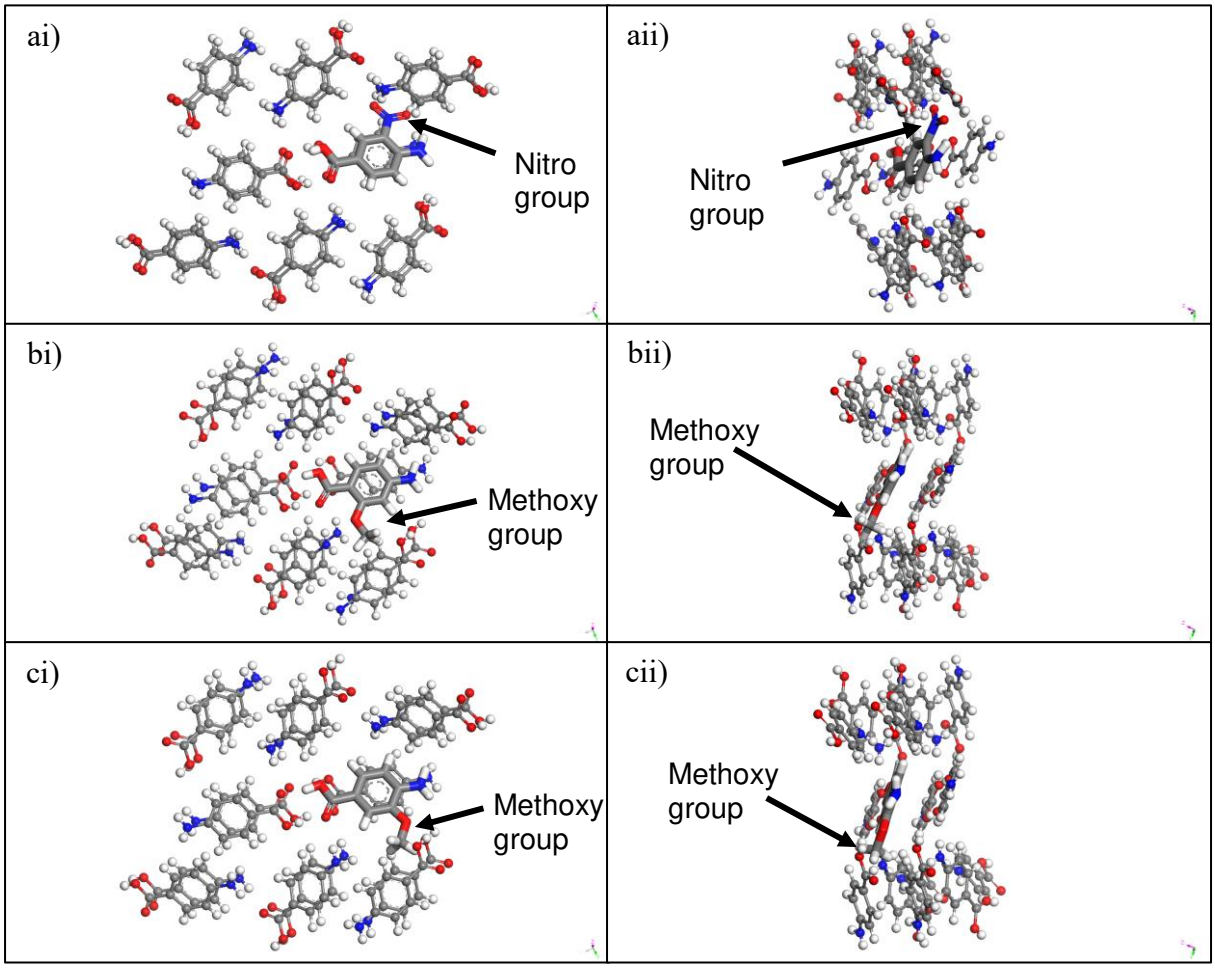

Figure 8. Visualisation of a) ANBA3, b) AMBA2 and c) AMBA3 within the pABA unit cell, based on the calculated strongest interaction geometry. i) View along b axis, ii) view along c axis. TMAs shown by thicker bonding molecules. Nitro and methoxy moieties would inhibit pABA molecules close to them from packing in the required pABA unit cell structure. Crystal structure taken from AMBNAC07 in CCDC[46].

The results of the intermolecular grid search pABA:TMA screen demonstrate that TMA selection should not be based solely on the molecular similarity of a target solute and an additive. This is still no guarantee of TMA competitive binding, shown by the comparison of

interaction energies of ANBA3 and ANBA2. Both molecules have the same moieties, but the nitro group is present on different carbons of the cyclic ring, with the nitro group on the second carbon (ortho position) for ANBA2 and the third carbon (meta position) for ANBA3. The group placement had a large effect on intermolecular interaction energy strengths with pABA. This suggests that the nitro group moiety placement on the molecular structure had a large influence on the molecular polarity and as such on interaction strengths. This would also suggest that ANBA3 would have a larger influence on the other intermolecular interactions important for pABA self-assembly than ANBA2.

3.5. Experimental Screening

An experimental screen of the crystallisation of pABA:pABA and pABA:TMAs from ethanol solution, using the same TMAs that were assessed through intermolecular grid search, was undertaken to validate the results obtained through the in silico TMA screen and to demonstrate TMA effectiveness in a real solution, with the influence of solvent molecules.

The effectiveness of each TMA to inhibit pABA nucleation was assessed through a study of T_c of each solution as a function of heating cycle rate, with a lowering of T_c assumed to correlate with nucleation inhibition. Figure 9 shows determined average T_c and T_{diss} results obtained for each solution studied. The experimental results corroborate the findings from the intermolecular grid search screen, with the most effective TMAs being found to be ANBA3, AMBA2 and AMBA3, decreasing T_c by an average of 24.0 °C, 9.4 °C and 6.7 °C, respectively. A student T-test statistical analysis was completed to determine if deviations in average values of T_c were statistically significant. Only the TMAs: ANBA3, AMBA2 and AMBA3 were found to have statistical significance when compared to results collected with pABA in ethanol solutions. The full student t-test analysis results are provided in Supplementary Information

S9. The variation in T_{diss} was found to be negligible with or without TMAs present, suggesting that the TMAs used had no significant effect on the solubility of pABA in ethanol. Dynamic MSZWs as a function of cooling rate were determined using the values of T_c and T_{diss} for each solution and are given in figure 9. These further highlight the effectiveness of ANBA3, AMBA2 and AMBA3 to inhibit pABA nucleation from ethanol solution given the increase in MSZW for these systems.

ANBA3 had the greatest effect on T_c, lowering it substantially more than any other TMA, demonstrating that the nitro group of ANBA3 had a larger effect on disrupting pABA nucleation than the methoxy group of AMBA2. This highlights the importance of not just synthon A, but also synthons B and C, given that the nitro group of ANBA3 would likely influence these intermolecular interaction more than the methoxy groups of AMBA2 and AMBA3, as discussed previously. This correlates with the intermolecular interaction energy calculations and the charge calculations of these moieties discussed previously, further validating the intermolecular grid search results. Overall, these results suggest that TMAs must competitively bind at least with equivalence to the host molecule but a second criterion is that the secondary interactions must disrupt the preassembly cluster formation, in order to inhibit the nucleation process.

It should also be noted that the growth rate of pABA was likely reduced by the presence of the TMAs that influenced its nucleation. ANBA3 and AMBA3 have previously been shown to reduce the growth rate of pABA in 2-propanol solution[27]. AMBA3 was found to have a more drastic effect on reducing growth rates at lower additive loadings, although the reduction in growth rates became similar at around 1 wt% loading. However, from figure 9 it is clear that ANBA3 had a larger effect on inhibiting nucleation than AMBA3. Therefore, the reduction in

growth rate would likely influence the detection of crystallites in solution and could contribute to the lowering of the solution crystallisation temperatures for the pABA:ANBA3, pABA:AMBA2 and pABA:AMBA3 solutions, but it is clear that there is a larger impact of the TMAs on the nucleation process.

In order to determine whether any polymorphic transformations had occurred as a result of the presence of the TMAs with the pABA in ethanol solution, a morphological assessment was completed. Previously, it has been found that the two most dominant pABA polymorphs, α-pABA and β-pABA, have distinct morphologies, being needle-like and prismatic, respectively. Furthermore, this morphological dissimilarity has been shown to still be present in the presence of TMAs[27]. All crystals collected from the crystallisation experiments undertaken during this study were found to conform to the needle-like morphology of α-pABA, therefore, no polymorphic transformations are presumed to have taken place. Optical micrographs showing crystals collected from experiments using all TMAs are provided in Supplementary Information S11.

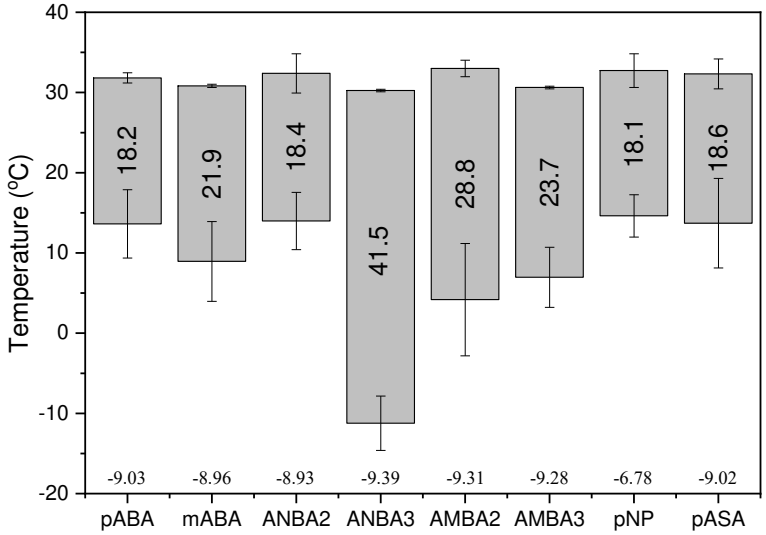

Figure 9. Floating column chart displaying T_c (bottom of columns) and T_{diss} (top of columns) values determined for pABA in ethanol solution with and without the presence of TMAs. Error bars show standard deviations of results. Numeric value within columns represents dynamic MSZW in °C. Values at bottom of plot are the strongest interaction energies for each dimer, calculated from the intermolecular grid search, in kcal mol^{-1}.

Due to the pABA nucleation inhibition from ethanol solution capabilities of ANBA3, this was the TMA that was further studied.

3.6. Mechanistic Understanding

3.6.1. Crystallisability and Solution Thermodynamics

Steady-state MSZW analysis highlighted the difference in crystallisability between pABA and pABA:ANBA3 in ethanol solutions. Over the concentration ranges studied the addition of ANBA3 increased the steady-state MSZW substantially, table 3. Negligible variations in the

trend of increasing equilibrium dissolution temperatures, T_e, with increasing solution concentration were determined, corroborating the previous finding of ANBA3 having a negligible effect on pABA solubility in ethanol. Therefore, the increase in the steady-state MSZW is attributed to the large decreases in the equilibrium crystallisation temperatures at the kinetic limit, $T_{c/l}$, observed. This demonstrates that pABA:ANBA3 required a much higher driving force to induce nucleation than for pABA in ethanol solution.

A van't Hoff analysis demonstrated a very similar trend, with regards to solution thermodynamics of the crystallising systems, with negligible changes in the enthalpy and entropy of dissolution between both systems found. Full results of the van't Hoff analysis are given in Supplementary Information S13.

Table 3. Equilibrium crystallisation and dissolution temperatures determined over a range of concentrations as well as steady-state MSZWs for pABA and pABA:ANBA3 in ethanol solutions.

Concentration (g g^{-1})	$T_{c/l}$	T_e	**MSZW (°C)**	**Concentration (g g^{-1})**	$T_{c/l}$	T_e	**MSZW (°C)**
pABA				**pABA:ANBA3**			
0.14	12.9	16.4	3.5	0.18	1.8	34.0	32.2
0.15	14.7	22.2	7.5	0.19	8.2	36.4	28.2
0.16	22.3	26.4	4.1	0.20	18.0	41.4	23.4
0.17	23.0	30.6	7.6	0.21	20.8	49.6	28.8

3.6.2. Nucleation Kinetics

The KBHR approach was used to determine the mechanism by which nucleation occurred and the nucleation kinetic parameters for pABA:ANBA3 in ethanol solutions. An example plot of u_c vs q in ln-ln coordinates, for nucleation mechanism assessment, for pABA:ANBA3 in ethanol solution at a concentration of 0.21 g g^{-1} is shown in figure 10.

Turner et al.[49] previously found that, over a comparable range of concentrations studied for pABA:ANBA3 in ethanol solutions, pABA in ethanol solutions nucleate through an IN pathway, table 4. Small angle X-ray studies have previously shown that the IN mechanism associated with pABA in ethanol solutions is mediated through the existence of pABA prenucleation clusters, which nucleate when a high enough driving force of supersaturation is reached[48]. This suggests an equilibrium of pABA clusters with similar energies exist in the supersaturated solution state, whereby once a high enough driving force to nucleation is achieved, given a high enough supersaturation, this equilibrium ensures a mechanistic nucleation pathway by which all nuclei reach a critical size in one instant, before subsequent crystal growth occurs.

In contrast, pABA:ANBA3 in ethanol solutions were found to undertake the PN pathway for all concentrations studied, table 4. This suggests that the equilibrium of cluster formation that could undergo nucleation at a given instance, present in pABA in ethanol solutions, was disrupted by the presence of ANBA3. From the in silico findings it is clear that there are strong pABA:ANBA3 intermolecular interactions and the presence of ANBA3 is able to direct non-crystallographic synthons, as well as providing steric hindrance to the formation of the pABA crystal structure. Therefore, this suggests that the presence of ANBA3 in solution disrupts the ability of solute clusters in solution to form into a pABA crystal structure. This result has been

found previously for TMA studies on nucleation inhibition of different crystallisation systems[24,26]. Therefore, it is assumed that a higher driving force to nucleation was required to overcome the favourable pABA:ANBA3 intermolecular interactions and remove the ANBA3 molecules from the clusters. Given the potential variation of clusters in solution, containing different numbers of ANBA3 and pABA molecules, only certain clusters would be provided with enough of a driving force to initiate the nucleation stage, once a critical nucleus size was reached, thereby altering the nucleation pathway to a state in which nucleation occurred in different areas of the solution over a period of time, in line with the PN pathway.

This novel insight into how ANBA3 affects the mechanism by which pABA nucleates from ethanol solution demonstrates that the interaction between the TMA and solute can fundamentally alter the behaviour of a nucleating system. Understanding how TMAs effect the mechanism of nucleation is extremely important as it can have a large impact on final crystal size distribution, solution hydrodynamics and system thermodynamics, etc.

Table 4. Nucleation mechanisms determined from slope of u_c vs q in ln-ln coordinates and calculated nucleation kinetic parameters obtained for pABA:ANBA3 in ethanol solutions from KBHR analysis. Data presented for pABA in ethanol solutions over a comparable concentration range, taken from Turner et al[49].

Concentration (g g^{-1})	**Slope**	**R^2 of linear fit**	**Mechanism**	γ_{eff} **(mJ m^{-2})**	r^* **(nm)**	i^*
pABA (from Turner et al.[49])						
0.18	1.76	0.80	IN	-	-	-
0.19	1.56	0.53	IN	-	-	-
0.20	1.62	0.62	IN	-	-	-

pABA:ANBA3						
0.18	9.18	0.91	PN	3.74	0.93 - 0.84	20.2 - 14.8
0.19	6.70	0.95	PN	2.98	0.83 - 0.72	14.5 - 9.5
0.20	3.95	0.96	PN	1.83	0.57 - 0.44	4.8 - 2.1
0.21	5.30	0.98	PN	2.59	0.74 - 0.60	10.1 - 5.5

For the PN case of pABA:ANBA3, the KBHR approach enabled the calculation of the nucleation kinetic parameters, γ_{eff}, r^* and i^*, shown in table 3. Plots of u_c vs ln q were formed and fitted with equation 5 to enable the determination of the parameters. An example of the u_c vs ln q plot for pABA:ANBA3 in ethanol solution at a concentration of 0.21 g g^{-1} is shown in figure 8.

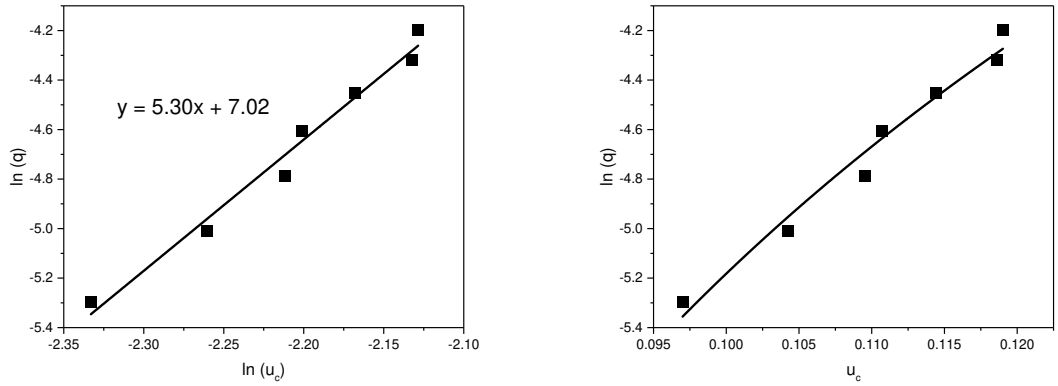

Figure 10. Plots for KBHR analysis for pABA:ANBA3 in ethanol solution at a concentration of 0.21 g g^{-1}. Left-hand side - Plot of u_c vs q in ln-ln coordinates for determination of nucleation mechanism. Right-hand side - Plot of u_c vs ln q for determination of nucleation kinetic parameters.

A previous research study determined values of γ_{eff} for pABA in ethanol solution using isothermal induction time data and CNT analysis[48]. Over a similar concentration range as studied in this work, the values of γ_{eff} were calculated to range from 0.85 - 1.31 mJ m^{-2}. In contrast values of γ_{eff} for pABA:ANBA3 in ethanol solution calculated from this analysis were found to be between 1.8 - 3.7 mJ m^{-2}. The higher γ_{eff} demonstrates that the presence of ANBA3 increased the required driving force to nucleation, which correlates well with the depression in T_c observed with experimental crystallisation studies as well as the nucleation mechanism change from IN to PN with the presence of ANBA3 in solution.

4. Conclusions

4.1. Conclusions of this Study

A workflow for TMA screening and assessment was developed and undertaken to study the nucleation inhibition effects of 7 TMAs on pABA crystallising from ethanol solution.

Intermolecular grid search results suggested that 3 out of 7 studied TMAs (ANBA3, AMBA2 and AMBA3) interacted more strongly with pABA than pABA did with itself. The other TMAs were found to have weaker intermolecular interactions. Therefore, ANBA3, AMBA2 and AMBA3 would likely form competitively to pABA in solution , forming through the important synthon A, whereas the others would have a much smaller influence on intermolecular interactions in solution.

These 3 pABA:TMA dimers were found to be more stable in solution than pABA:pABA dimers and as such, harder to desolvate. pABA:ANBA3 was also found to likely disrupt the important synthon C formation necessary for pABA nucleation. Atomic fractional charges

demonstrated that ANBA3 would have stronger intermolecular interactions with subsequent pABA molecules due to strong charges on its nitro and amine groups and TMA cyclic rings had varied charges, suggesting an ability to alter synthon B and C formation. All 3 pABA:TMA dimers were found to be unlikely to fit within the pABA crystal structure and as such, would be likely to disrupt the important synthon B and other pABA intermolecular interactions necessary for pABA nucleation. Therefore, although initial in silico testing provided an indication as to the likely interaction strengths of pABA homodimers and pABA:TMA heterodimers, through assessment of the impact of TMAs on key pABA synthons (A, B and C), stability of dimers in solution, subsequent pABA interactions, atomic fractional charges and the stereochemistry associated with TMA incorporation into the crystal structure, the impact of the TMAs on pABA nucleation was comprehensively evaluated.

Experimental screening corroborated the in silico findings, with only ANBA3, AMBA2 and AMBA3 having an ability to lower the crystallisation temperature of pABA in ethanol solution. ANBA3 was found to have the largest nucleation inhibition effect.

The crystallisability, solution thermodynamics and nucleation kinetics of pABA:ANBA3 were assessed to gain a mechanistic understanding of TMA inhibition of pABA nucleation. Large increases were observed in the steady-state MSZW with the presence of ANBA3 in solution, with little changes in the solution thermodynamics. The mechanism of nucleation was found to change from instantaneous nucleation for pABA in ethanol solution to progressive nucleation in the presence of ANBA3 in solution. This is suggested to be as a result of ANBA3 molecules influencing the ability of pABA molecules to form into their crystal structure to enable the nucleation process to occur. A higher driving force to nucleation would be needed for ANBA3 to be removed from these clusters and allow pABA nucleation to occur. This was

found to be the case, with a higher supersaturation necessary to induce nucleation of pABA:ANBA3 in ethanol solutions, as well as a higher effective interfacial tension calculated for these solutions.

4.2. Applications, Future Work and Current Limitations

Industrial additive selection can take the form of an initial selection of hundreds of potentially useful additives followed by an additive screen to determine the most effective. This is a long and tedious process that requires substantial experimental effort and money to complete. Furthermore, these screens provide no real information as to the mechanism of action of the additives towards the crystallisation process, which means fundamental knowledge cannot be used to aid future additive selection. The workflow produced in this study provides a step towards making the process of additive selection, as well as understanding fundamental mechanistic additive influences on the crystallisation process, more efficient, by reducing experimental expenditure and gaining greater insights to aid in future idea generation.

The workflow produced could also be implemented towards understanding how chemical synthesis impurities effect the crystallisation of desired products. This is due to these impurities being akin to TMAs, i.e. they have a similar molecular structure to the desired product. This could then aid in process understanding so that process parameters, such as solvent selection, could be altered. This could potentially change intermolecular interaction pathways to nucleation, creating a more controlled crystallisation process.

Furthermore, although not thoroughly discussed in this work, understanding how TMAs interact with preassembly/nucleation pathways can aid in directing polymorphic form. This has been shown in a previous study by Black et al.[27], whereby, at higher additive loadings and

higher solution volumes to those used in this work, ANBA3 and AMBA3 were able to direct the crystallisation of β-pABA, with explanations given as to the TMAs interfering with the important synthons in α-pABA crystal structure. The workflow presented here provides a way in which to thoroughly understand these interactions and as such could be used to aid polymorphic form selectivity.

A limitation of this work is that it does not address key issues arising from TMA studies, such as understanding how TMA concentration influences nucleation inhibition or how changes in TMA solubility in the solvent influence its efficacy.

A further limitation of this work is that it focusses upon a relatively simple molecule in a model crystallisation system. Therefore, it does not take into account added complexity of many solutions. This complexity could be the result of many factors, such as high molecular weight compounds, highly charged compounds, multi component systems, lower purity products or hydrophobic systems that do not have strong hydrogen bonding responsible for key synthons.

In order to ensure effective workflow procedures and universal applicability, it is suggested that the produced workflow should be developed and validated further, through subsequent studies on nucleation inhibition using TMAs of different systems. With further studies and successive methodological improvement it is suggested that the TMA selection workflow could become a more common and rigorously used industrial crystallisation tool.

Supporting Information

The Supporting Information is available free of charge.

It includes: pABA crystallisation background science, grid optimization, intermolecular interaction energies and contributions, dimer interaction geometries, dimer solvation and pABA interaction energies, TMAs within pABA crystal structure, statistical T-test, TMA screen MSZWs, pABA optical micrographs, crystallisation and dissolution temperatures, crystallisability and van't Hoff analysis and nucleation kinetic analysis.

Corresponding Author

Kevin J. Roberts - EPSRC Centre for Doctoral Training in Complex Particulate Products and Processes School of Chemical and Process Engineering, University of Leeds, Leeds, UK.

Email – K.J.Roberts@leeds.ac.uk

Notes

The authors declare no competing financial interest

Acknowledgements

This research, which forms part of the doctoral studies of one of us (PLK), was carried out at the EPSRC Centre for Doctoral Training in Complex Particulate Products and Processes (EP/L015285/1) as part of a collaborative project with Infineum Ltd. And Syngenta Ltd., who we gratefully acknowledge. The grid-search software used in this research forms part of the Synthonic Engineering Toolset developed through the Advanced Manufacturing Supply Chain Initiative (Advanced Digital Design of Pharmaceutical Therapeutics (ADDoPT): Grant No. 14060). This work also builds upon the Synthonic Engineering Program supported by the EPSRC (Grant EP/I028293/1) in collaboration with Pfizer, Boeringer-Ingellheim, Novartis and

Syngenta. The research on the pABA system also builds upon a collaborative EPSRC Critical Mass programme (Molecules, Clusters and Crystals: Grant EP/I014446/1 and EP/I013563/1) with the University of Manchester.

References

(1) Kaskiewicz, P. L.; Xu, G.; Lai, X.; Warren, N. J.; Roberts, K. J.; Morton, C.; Dowding, P.; George, N. Isothermal by Design: An Accelerated Approach to the Prediction of the Crystallizability of Slowly Nucleating Systems. *Org. Process Res. Dev.* **2019**, *23* (9), 1948–1959. https://doi.org/10.1021/acs.oprd.9b00242.

(2) Tang, X.; Kaskiewicz, P. L.; Camacho Corzo, D. M.; Lai, X.; Roberts, K. J.; Dowding, P.; More, I. Solubility and Crystallisability of the Ternary System: Hexadecane and Octadecane Representative in Fuel Solvents. *Fuel* **2018**, *226*, 665–674.

(3) Gracin, S.; Rasmuson, Å. C. Polymorphism and Crystallization of P-Aminobenzoic Acid. *Cryst. Growth Des.* **2004**, *4* (5), 1013–1023. https://doi.org/10.1021/cg049954h.

(4) Simone, E.; Steele, G.; Nagy, Z. K. Tailoring Crystal Shape and Polymorphism Using Combinations of Solvents and a Structurally Related Additive. *CrystEngComm* **2015**, *17* (48), 9370–9379. https://doi.org/10.1039/c5ce01878a.

(5) Simone, E.; Saleemi, A. N.; Tonnon, N.; Nagy, Z. K. Active Polymorphic Feedback Control of Crystallization Processes Using a Combined Raman and ATR-UV/Vis Spectroscopy Approach. *Cryst. Growth Des.* **2014**, *14* (4), 1839–1850.

(6) Rosbottom, I.; Ma, C. Y.; Turner, T. D.; O'Connell, R. A.; Loughrey, J.; Sadiq, G.; Davey, R. J.; Roberts, K. J. Influence of Solvent Composition on the Crystal Morphology and Structure of P-Aminobenzoic Acid Crystallized from Mixed Ethanol

and Nitromethane Solutions. *Cryst. Growth Des.* **2017**, *17* (8), 4151–4161.

(7) Sangwal, Mk. *Additives and Crystallization Processes: From Fundamentals to Applications*; John Wiley & Sons Ltd.: Chichester, 2007.

(8) Buckley, H. E. Some New Features in Habit-Modification Shown by KClO4 Crystals. *Zeitschrift für Krist.* **1935**, *91* (1), 375. https://doi.org/https://doi.org/10.1524/zkri.1935.91.1.375.

(9) Buckley, H. E. Habit Modification in Crystals as a Result of the Introduction of Impurities during Growth. *Discuss. Faraday Soc.* **1949**, *5* (7), 243–254. https://doi.org/10.1039/DF9490500243.

(10) Butchart, A.; Whetstone, J. The Effect of Dyes on the Crystal Habits of Some Oxy-Salts. *Discuss. Faraday Soc.* **1949**, *5*, 254–261. https://doi.org/10.1039/DF9490500254.

(11) Whetstone, J. The Effect of Crystal Habit Modification on the Setting of Inorganic Oxy-Salts. *Discuss. Faraday Soc.* **1949**, *5*, 261–266. https://doi.org/10.1039/DF9490500261.

(12) van Mil, J.; Gati, E.; Addadi, L.; Lahav, M. Useful Impurities for Optical Resolutions. 1. On the Crystallization of Photopolymerizing Dienes in the Presence of Their Chiral Topochemical Products. *J. Am. Chem. Soc.* **1981**, *103* (5), 1248–1249. https://doi.org/10.1021/ja00395a058.

(13) Addadi, L.; van Mil, J.; Lahav, M. Useful Impurities for Optical Resolutions. 2. Generality and Mechanism of the Rule of Reversal. *J. Am. Chem. Soc.* **1981**, *103* (5), 1249–1251. https://doi.org/10.1021/ja00395a059.

(14) Addadi, L.; Berkovitch Yellin, Z.; Domb, N.; Gati, E.; Lahav, M.; Leiserowitz, L. Resolution of Conglomerates by Stereoselective Habit Modifications. *Nature* **1982**, *296*

(5852), 21–26. https://doi.org/10.1038/296021a0.

(15) Wireko, F. C.; Shimon, L. J. W.; Frolow, F.; Berkovitch-Yellin, Z.; Lahav, M.; Leiserowitz, L. Effect of Solvent on the Growth of Organic Crystals. 1. The Riddle of α-Resorcinol. *J. Phys. Chem.* **1987**, *91* (2), 472–481. https://doi.org/10.1021/j100286a042.

(16) Weissbuch, I.; Addadi, L.; Lahav, M.; Leiserowitz, L. Molecular Recognition at Crystal Interfaces Reduction in Crystal Symmetry of Solid. *Science (80-.).* **1991**, *253* (September), 637–645. https://doi.org/10.1126/science.253.5020.637.

(17) Weissbuch, I.; Lahav, M.; Leiserowitz, L. Toward Stereochemical Control, Monitoring, and Understanding of Crystal Nucleation. *Cryst. Growth Des.* **2003**, *3* (2), 125–150. https://doi.org/10.1021/cg0200560.

(18) Clydesdale, G.; Roberts, K. J.; Lewtas, K.; Docherty, R. Modelling the Morphology of Molecular Crystals in the Presence of Disruptive Tailor-Made Additives. *J. Cryst. Growth* **1994**, *135* (1–2), 331–340. https://doi.org/10.1016/0022-0248(94)90250-X.

(19) Clydesdale, G.; Roberts, K. J.; Lewtas, K.; Docherty, R. Modelling the Morphology of Molecular Crystals in the Presence of Blocking Tailor-Made Additives. *J. Cryst. Growth* **1994**, *141* (3–4), 443–450. https://doi.org/10.1016/0022-0248(94)90250-X.

(20) Clydesdale, G.; Hammond, R. B.; Ramachandran, V.; Roberts, K. J.; Mougin, P. Molecular Modelling of the Morphology of Organic Crystals in the Presence of Impurity Species: Recent Applications to Naphthalene, Phenanthrene, and Caprolactam Crystals. *Mol. Cryst. Liq. Cryst.* **2005**, *440*, 235–257. https://doi.org/10.1080/15421400590958566.

(21) Black, S. N.; Davey, R. J.; Halcrow, M. The Kinetics of Crystal Growth in the Presence of Tailor-Made Additives. *J. Cryst. Growth* **1986**, *79* (1-3 PART 2), 765–774. https://doi.org/10.1016/0022-0248(86)90552-X.

(22) Chen, B. D.; Garside, J.; Davey, R. J.; Maginn, S. J.; Matsuoka, M. Growth of M-Chloronitrobenzene Crystals in the Presence of Tailor-Made Additives: Assignment of the Polar Axes from Morphological Calculations. *J. Phys. Chem.* **1994**, *98* (12), 3215–3221. https://doi.org/10.1021/j100063a027.

(23) Dowling, R.; Davey, R. J.; Curtis, R. A.; Han, G.; Poornachary, S. K.; Chow, P. S.; Tan, R. B. H. Acceleration of Crystal Growth Rates: An Unexpected Effect of Tailor-Made Additives. *Chem. Commun.* **2010**, *46* (32), 5924–5926. https://doi.org/10.1039/c0cc00336k.

(24) Heffernan, C.; Ukrainczyk, M.; Zeglinski, J.; Hodnett, B. K.; Rasmuson, Å. C. Influence of Structurally Related Impurities on the Crystal Nucleation of Curcumin. *Cryst. Growth Des.* **2018**, *18* (8), 4715–4723.

(25) Pons Siepermann, C. A.; Huang, S.; Myerson, A. S. Nucleation Inhibition of Benzoic Acid through Solution Complexation. *Cryst. Growth Des.* **2017**, *17* (5), 2646–2653. https://doi.org/10.1021/acs.cgd.7b00160.

(26) Pons Siepermann, C. A.; Myerson, A. S. Inhibition of Nucleation Using a Dilute, Weakly Hydrogen-Bonding Molecular Additive. *Cryst. Growth Des.* **2018**, *18*, acs.cgd.8b00367. https://doi.org/10.1021/acs.cgd.8b00367.

(27) Black, J. F. B.; Cruz-Cabeza, A. J.; Davey, R. J.; Willacy, R. D.; Yeoh, A. The Kinetic Story of Tailor-Made Additives in Polymorphic Systems: New Data and Molecular Insights for p-Aminobenzoic Acid. *Cryst. Growth Des.* **2018**, *18* (12), 7518–7525.

https://doi.org/10.1021/acs.cgd.8b01325.

(28) Ulrich, J. Solution Crystallization - Developments and New Trends. *Chem. Eng. Technol.* **2003**, *26* (8), 832–835. https://doi.org/10.1002/ceat.200300003.

(29) Mougin, P.; Clydesdale, G.; Hammond, R. B.; Roberts, K. J. Molecular and Solid-State Modeling of the Crystal Purity and Morphology of ε-Caprolactam in the Presence of Synthesis Impurities and the Imino-Tautomeric Species Caprolactim. *J. Phys. Chem. B* **2003**, *107* (48), 13262–13272. https://doi.org/10.1021/jp034350u.

(30) Hammond, R. B.; Ma, C.; Roberts, K. J.; Ghi, P. Y.; Harris, R. K. Application of Systematic Search Methods to Studies of the Structures of Urea-Dihydroxy Benzene Cocrystals. *J. Phys. Chem. B* **2003**, *107* (42), 11820–11826. https://doi.org/10.1021/jp035010b.

(31) Clydesdale, G.; Hammond, R. B.; Roberts, K. J. Molecular Modeling of Bulk Impurity Segregation and Impurity-Mediated Crystal Habit Modification of Naphthalene and Phenanthrene in the Presence of Heteroimpurity Species. *J. Phys. Chem. B* **2003**, *107* (20), 4826–4833. https://doi.org/10.1021/jp022423o.

(32) Harris, R. K.; Ghi, P. Y.; Hammond, R. B.; Ma, C. Y.; Roberts, K. J.; Yates, J. R.; Pickard, C. J. Solid-State NMR and Computational Studies of 4-Methyl-2-Nitroacetanilide. *Magn. Reson. Chem.* **2006**, *44* (3 SPEC. ISS.), 325–333. https://doi.org/10.1002/mrc.1779.

(33) Hammond, R. B.; Hashim, R. S.; Ma, C.; Roberts, K. J. Grid-Based Molecular Modeling for Pharmaceutical Salt Screening: Case Example of 3,4,6,7,8,9-Hexahydro-2H-Pyrimido (1,2-a) Pyrimidinium Acetate. *J. Pharm. Sci.* **2006**, *95* (11), 2361–2372. https://doi.org/10.1002/jps.20657.

(34) Ramachandran, V.; Murnane, D.; Hammond, R. B.; Pickering, J.; Roberts, K. J.; Soufian, M.; Forbes, B.; Jaffari, S.; Martin, G. P.; Collins, E.; Pencheva, K. Formulation Pre-Screening of Inhalation Powders Using Computational Atom-Atom Systematic Search Method. *Mol. Pharm.* **2015**, *12* (1), 18–33. https://doi.org/10.1021/mp500335w.

(35) Rosbottom, I.; Pickering, J. H.; Etbon, B.; Hammond, R. B.; Roberts, K. J. Examination of Inequivalent Wetting on the Crystal Habit Surfaces of RS-Ibuprofen Using Grid-Based Molecular Modelling. *Phys. Chem. Chem. Phys.* **2018**, *20* (17), 11622–11633. https://doi.org/10.1039/c7cp08354h.

(36) Rosbottom, I.; Pickering, J.; Hammond, R. B.; Roberts, K. J. A Digital Workflow Supporting the Selection of Solvents for Optimising the Crystallisability of Para Aminobenzoic Acid. *Org. Process Res. Dev.* **2020**, *24* (4), 500–507. https://doi.org/10.1021/acs.oprd.9b00261.

(37) Kashchiev, D.; Borissova, A.; Hammond, R. B.; Roberts, K. J. Effect of Cooling Rate on the Critical Undercooling for Crystallization. *J. Cryst. Growth* **2010**, *312* (5), 698–704. https://doi.org/10.1016/j.jcrysgro.2009.12.031.

(38) Kashchiev, D.; Borissova, A.; Hammond, R. B.; Roberts, K. J. Dependence of the Critical Undercooling for Crystallization on the Cooling Rate. *J. Phys. Chem. B* **2010**, *114* (16), 5441–5446. https://doi.org/10.1021/jp100202m.

(39) Camacho Corzo, D. M.; Borissova, A.; Hammond, R. B.; Kashchiev, D.; Roberts, K. J.; Lewtas, K.; More, I. Nucleation Mechanism and Kinetics from the Analysis of Polythermal Crystallisation Data: Methyl Stearate from Kerosene Solutions. *CrystEngComm* **2014**, *16* (6), 974–991.

(40) Svärd, M.; Nordström, F. L.; Hoffmann, E. M.; Aziz, B.; Rasmuson, Å. C.

Thermodynamics and Nucleation of the Enantiotropic Compound P-Aminobenzoic Acid. *CrystEngComm* **2013**, *15* (25), 5020–5031. https://doi.org/10.1039/c3ce26984a.

(41) Black, J. F. B.; Davey, R. J.; Gowers, R. J.; Yeoh, A. Ostwald's Rule and Enantiotropy: Polymorph Appearance in the Crystallisation of p-Aminobenzoic Acid. *CrystEngComm* **2015**, *17* (28), 5139–5142. https://doi.org/10.1039/c5ce00353a.

(42) Turner, T. D.; Caddick, S.; Hammond, R. B.; Roberts, K. J.; Lai, X. Kinetics of the Aqueous-Ethanol Solution Mediated Transformation between the Beta and Alpha Polymorphs of p-Aminobenzoic Acid. *Cryst. Growth Des.* **2018**, *18* (2), 1117–1125. https://doi.org/10.1021/acs.cgd.7b01551.

(43) Black, J. F. B.; Cardew, P. T.; Cruz-Cabeza, A. J.; Davey, R. J.; Gilks, S. E.; Sullivan, R. A. Crystal Nucleation and Growth in a Polymorphic System: Ostwald's Rule,: P - Aminobenzoic Acid and Nucleation Transition States. *CrystEngComm* **2018**, *20* (6), 768–776. https://doi.org/10.1039/c7ce01960b.

(44) Cruz-Cabeza, A. J.; Davey, R. J.; Oswald, I. D. H.; Ward, M. R.; Sugden, I. J. Polymorphism in P-Aminobenzoic Acid. *CrystEngComm* **2019**, *21* (13), 2034–2042. https://doi.org/10.1039/C8CE01890A.

(45) Rosbottom, I.; Roberts, K. J.; Docherty, R. The Solid State, Surface and Morphological Properties of p-Aminobenzoic Acid in Terms of the Strength and Directionality of Its Intermolecular Synthons. *CrystEngComm* **2015**, *17* (30), 5768–5788. https://doi.org/10.1039/c5ce00302d.

(46) Sullivan, R. A.; Davey, R. J. Concerning the Crystal Morphologies of the α and β Polymorphs of P-Aminobenzoic Acid. *CrystEngComm* **2015**, *17* (5), 1015–1023. https://doi.org/10.1039/c4ce01857e.

(47) Sullivan, R. A.; Davey, R. J.; Sadiq, G.; Dent, G.; Back, K. R.; Ter Horst, J. H.; Toroz, D.; Hammond, R. B. Revealing the Roles of Desolvation and Molecular Self-Assembly in Crystal Nucleation from Solution: Benzoic and p -Aminobenzoic Acids. *Cryst. Growth Des.* **2014**, *14* (5), 2689–2696.

(48) Toroz, D.; Rosbottom, I.; Turner, T. D.; Corzo, D. M. C.; Hammond, R. B.; Lai, X.; Roberts, K. J. Towards an Understanding of the Nucleation of Alpha-Para Amino Benzoic Acid from Ethanolic Solutions: A Multi-Scale Approach. *Faraday Discuss.* **2015**, *179*, 79–114.

(49) Turner, T. D.; Corzo, D. M. C.; Toroz, D.; Curtis, A.; Dos Santos, M. M.; Hammond, R. B.; Lai, X.; Roberts, K. J. The Influence of Solution Environment on the Nucleation Kinetics and Crystallisability of Para-Aminobenzoic Acid. *Phys. Chem. Chem. Phys.* **2016**, *18* (39), 27507–27520.

(50) Davey, R. J.; Back, K. R.; Sullivan, R. A. Crystal Nucleation from Solutions - Transition States, Rate Determining Steps and Complexity. *Faraday Discuss.* **2015**, *179*, 9–26. https://doi.org/10.1039/c5fd00037h.

(51) Cruz-cabeza, A. J.; Davey, R. J.; Sachithananthan, S. Aromatic Stacking - a Key Step in Nucleation. *Chem. Commun.* **2017**, *53*, 7905–7908. https://doi.org/10.1039/C7CC02423A.

(52) Rosbottom, I.; Toroz, D.; Hammond, R. B.; Roberts, K. J. Conformational and Structural Stability of the Single Molecule and Hydrogen Bonded Clusters of Para Aminobenzoic Acid in the Gas and Solution Phases. *CrystEngComm* **2018**, *20* (46), 7543–7555. https://doi.org/10.1039/c8ce00908b.

(53) Nappo, V.; Sullivan, R.; Davey, R.; Kuhn, S.; Gavriilidis, A.; Mazzei, L. Effect of Shear

Rate on Primary Nucleation of Para-Amino Benzoic Acid in Solution under Different Fluid Dynamic Conditions. *Chem. Eng. Res. Des.* **2018**, *136*, 48–56. https://doi.org/10.1016/j.cherd.2018.04.039.

(54) Rosbottom, I.; Roberts, K. J. Crystal Growth and Morphology of Molecular Crystals. In *Engineering Crystallography: From Molecule to Crystal to Functional Form. NATO Science for Peace and Security Series A: Chemistry and Biology*; Roberts, K. J., Docherty, R., Tamura, R., Eds.; Springer: Dordrecht, 2017; pp 109–131.

(55) Roberts, K. J.; Hammond, R. B.; Ramachandran, V.; Docherty, R. Synthonic Engineering. In *Computational Pharmaceutical Solid State Chemistry*; Abramov, Y. A., Ed.; John Wiley & Sons, Ltd, 2016; pp 175–210. https://doi.org/https://doi.org/10.1002/9781118700686.ch8.

(56) The Cambridge Crystallographic Data Centre. Cambridge Structural Database https://www.ccdc.cam.ac.uk/solutions/csd-system/components/csd/.

(57) Mayo, S. L.; Olafson, B. D.; Goddard, W. A. DREIDING: A Generic Force Field for Molecular Simulations. *J. Phys. Chem.* **1990**, *94* (26), 8897–8909. https://doi.org/10.1021/j100389a010.

(58) Becke, A. D. A New Mixing of Hartree-Fock and Local Density-Functional Theories. *J. Chem. Phys.* **1993**, *98* (2), 1372–1377. https://doi.org/10.1063/1.464304.

(59) Lee, C.; Yang, W.; Parr, R. G. Development of the Colle-Salvetti Correlation-Energy Formula into a Functional of the Electron Density. *Phys. Rev. B* **1988**, *37* (2), 785–789. https://doi.org/10.1103/PhysRevB.37.785.

(60) Frisch, M. J.; Trucks, G. W.; Schlegel, H. B.; Scuseria, G. E.; Robb, M. A.; Cheeseman,

J. R.; Scalmani, G.; Barone, V.; Petersson, G. A.; Nakatsuji, H.; Li, X.; Caricato, M.; Marenich, A.; Bloino, J.; Janesko, B. G.; Gomperts, R.; Mennucci, B.; Hratchian, H. P.; Ortiz, J. V.; Izmaylov, A. F.; Sonnenberg, J. L.; Williams-Young, D.; Ding, F.; Lipparini, F.; Egidi, F.; Goings, J.; Peng, B.; Petrone, A.; Henderson, T.; Ranasinghe, D.; Zakrzewski, V. G.; Gao, J.; Rega, N.; Zheng, G.; Liang, W.; Hada, M.; Ehara, M.; Toyota, K.; Fukuda, R.; Hasegawa, J.; Ishida, M.; Nakajima, T.; Honda, Y.; Kitao, O.; Nakai, H.; Vreven, T.; Throssell, K.; Montgomery Jr., J. A.; Peralta, J. E.; Ogliaro, F.; Bearpark, M.; Heyd, J. J.; Brothers, E.; Kudin, K. N.; Staroverov, V. N.; Keith, T.; Kobayashi, R.; Normand, J.; Raghavachari, K.; Rendell, A.; Burant, J. C.; Iyengar, S. S.; Tomasi, J.; Cossi, M.; Millam, J. M.; Klene, M.; Adamo, C.; Cammi, R.; Ochterski, J. W.; Martin, R. L.; Morokuma, K.; Farkas, O.; Foresman, J. B.; Fox, D. J. Gaussian09, Revision D.01. Gaussian, Inc.: Wallingford CT 2016.

(61) BIOVIA Dassault Systèmes. Materials Studio https://www.3dsbiovia.com/portfolio/materials-studio.html.

(62) Gasteiger, J.; Marsili, M. A New Model for Calculating Atomic Charges in Molecules. *Tetrahedron Lett.* **1978**, *19* (34), 3181–3184. https://doi.org/10.1016/S0040-4039(01)94977-9.

(63) Gasteiger, J.; Marsili, M. Iterative Partial Equalization of Orbital Electronegativity-a Rapid Access to Atomic Charges. *Tetrahedron* **1980**, *36* (22), 3219–3228. https://doi.org/10.1016/0040-4020(80)80168-2.

(64) Technobis. Crystal16 https://www.crystallizationsystems.com/crystal16.

(65) Hildebrand, J. H.; Jenks, C. A. Solubility. IV. Solubility Relations of Naphthalene and Iodine in the Various Solvents, Including a Method for Evaluating Solubility Data. *J.*

Am. Chem. Soc. **1920**, *42* (11), 2180–2189. https://doi.org/10.1021/ja01456a008.

(66) Grant, D. J. W.; Mehdizadeh, M.; Chow, A. H. L.; Fairbrother, J. E. Non-Linear van't Hoff Solubility-Temperature Plots and Their Pharmaceutical Interpretation. *Int. J. Pharm.* **1984**, *18* (1–2), 25–38. https://doi.org/10.1016/0378-5173(84)90104-2.

(67) Turner, T. D. Molecular Self-Assembly, Nucleation Kinetics and Cluster Formation Associated with Solution Crystallisation, University of Leeds, 2015.